

Temperature-to-Frequency Converter With 1.47% Error Using Thermistor Linearity Calibration

Chua-Chin Wang¹, Senior Member, IEEE, Zong-You Hou, and Jih-Cheng You

Abstract—Temperature variation is well known to be very critical for estimating other parameters, e.g., the state of charge and the state of health of batteries. A high-accuracy temperature to frequency converter with thermistor linear calibration based on the thermistor linearization circuit is designed and analyzed in this investigation, where a voltage-to-frequency converter (VFC) is added instead of an analog-to-digital converter. The proposed design converts the voltage into a digital signal (frequency output) to reduce design complexity as well as the cost of chip area. A detailed analysis, including the method using the thermistor linearization calibration circuit and VFC, is reported in this paper. The measurement results in a thermal chamber establish that the output frequency is 1.62 to 2.27 MHz, the maximum linearity error is $\pm 0.5\%$, and the temperature error is $\leq 1.47\%$ in the temperature range of 268.15 to 313.15 K.

Index Terms—Thermistor, temperature variation, sensitivity, VFC, linear calibration.

I. INTRODUCTION

SMART electronic products are often equipped with many sensors to carry out specific functions, e.g., voltage, current, or temperature sensing, at a given time. Temperature is considered to be one of the most important parameters. For instance, high temperature usually results in higher power consumption and even system breakdown.

Many temperature sensing methods are used in industrial applications, including the thermocouple, resistance thermometer, infrared spectrum, and thermistor. The thermocouple is an electrical device consisting of two dissimilar electrical conductors with different temperature coefficients forming an electrical junction. If the conductors are used, the electrical device will generate a weak voltage. When the temperature of one conductor is measured, the temperature of the other conductor can be derived from the weak voltage according to the Seebeck effect. Although the resistance thermometer has been used for temperature measurement, the measured resistance is not accurate enough due to its poor sensitivity. The

Manuscript received November 6, 2018; revised January 30, 2019; accepted March 3, 2019. Date of publication March 8, 2019; date of current version June 4, 2019. This work was supported by the Ministry of Science and Technology under Grant MOST 107-2218-E-110-004 and Grant MOST 107-2218-E-110-016. This work was also partially supported by the National Sun Yat-sen University under Grant 08TPL01 and chip fabrication by CIC (Chip Implementation Center) of NARL (Nation Applied Research Laboratories), Taiwan. The associate editor coordinating the review of this paper and approving it for publication was Prof. Zeljko Ignjatovic. (Corresponding author: Chua-Chin Wang.)

The authors are with the Department of Electrical Engineering, National Sun Yat-sen University, Kaohsiung 80424, Taiwan (e-mail: ccwang@ee.nsysu.edu.tw).

Digital Object Identifier 10.1109/JSEN.2019.2903713

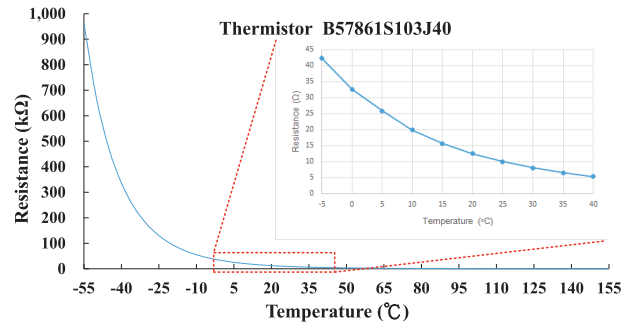


Fig. 1. Thermistor characteristic [1], [2].

infrared thermometer utilizes the infrared spectrum to measure the temperature. The sensing principle of the thermistor is very similar to that of the resistance thermometer, but the material is mainly composed of ceramic polymer. Thus, the reaction is faster and the volume is also smaller. Table I compares the above four temperature detection methods.

Thermistors having features such as ruggedness, high sensitivity, accuracy and low cost are often used for cost-effective usage in industry. However, the thermistor sensor has a serious flaw, namely, a highly nonlinear resistance-temperature characteristic as shown in Fig. 1 [1], [2]. Many researchers have focused on resolving this issue, e.g., [3], [4]. Sarkar *et al.* [4] use an inverting operational amplifier with a linear correction resistor to correct the thermistor. The advantage of this method is the simple implementation. However, the sensing temperature range is too wide, and the resistance of the linear correction resistor does not vary moderately with temperature so that the maximum error is 3% at the lowest and highest temperatures. In addition, the amplifier is a commercially component with dual power supply, which makes the overall circuit large and complicated.

Fig. 2 shows a linearization scheme for thermistor-based sensing in biomedical applications [5]. The oscillator frequency varies with the temperature. The resistance (r) is used to calibrate the linearity of the circuit. The resistance value of r is selected on the basis of Eqn. (1):

$$r = \frac{R_{TM}(R_{TL}R_{TM} + R_{TM}R_{TU} - 2R_{TL}R_{TU})}{2(R_{TL}R_{TU} - R_{TM}^2)} \quad (1)$$

where R_{TU} is the resistance of the thermistor at the highest selected temperature, R_{TL} is the resistance of the thermistor at the lowest selected temperature, and R_{TM} is the resistance of the thermistor at the center temperature. The output frequency

TABLE I
THE COMPARISON TABLE OF THE TEMPERATURE DETECTION METHODS

	Thermocouple	Resistance thermometer	Infrared	Thermistor
Sensing temperature range(°C)	-200~1200	-200~500	-50~400	-90~150
Volume (mm)	≈0.20×2000	≈0.10×2000	≈200×50×50	≈0.5×1
Reaction	fast	slow	fast	fast
Flexibility	none	none	none	yes
Disadvantage	Need a reference temperature	Expensive	Limited measurement method	Nonlinear

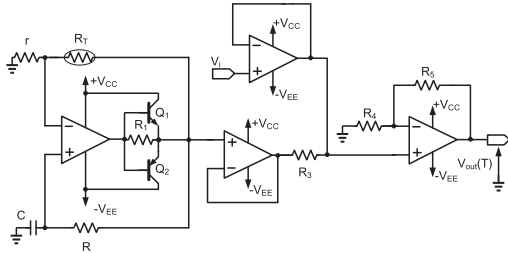


Fig. 2. Linearization scheme for thermistor-based sensing in biomedical applications [5].

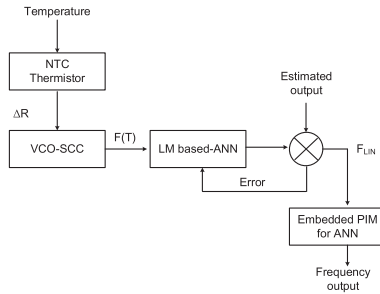


Fig. 3. Block diagram of an ANN-based linearization technique for the VCO thermistor circuit [6].

is derived as follows:

$$\text{Frequency of } V_{out}(T) = \frac{1}{2RC \cdot \ln(1 + \frac{2r}{R_T})} \quad (2)$$

where R, C, and R_T are shown in Fig. 2.

Because the output frequency is used to denote the output, data error caused by noise with long-distance transmission can be avoided. However, this circuit has too many resistors resulting in a large output error due to resistance variations.

Fig. 3 shows the block diagram of a neural-network-based method [6]. The neural network calculates the weights and biases of different thermistors and transmits them to the LM based-ANN. Thus, $F(T)$ is linearly corrected to F_{LIN} in accordance with the weights and biases. The simulation results of this work are very impressive. However, this design requires an additional computer, which is hard to integrate into a portable system to calculate parameters and frequency correction. It is extremely inconvenient in a space-limited scenario.

Nenova and Nenov [7] proposed a temperature sensor comprising a 7555 timer with a thermistor (R_T) as shown in Fig. 4. R_T varies with temperature, and the output frequency (f) timer

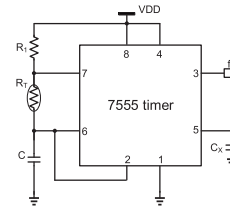


Fig. 4. Temperature sensor composed of a 7555 timer and a thermistor [7].

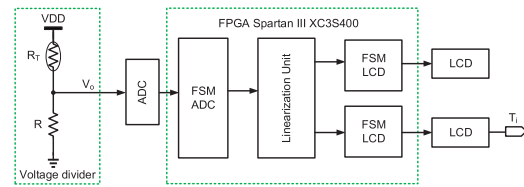


Fig. 5. Thermistor sensor by piecewise linear interpolation in FPGA [8].

varies with R_T . Therefore, f is written as follows:

$$f = \frac{1.44}{C(R_1 + 2R_T)} \quad (3)$$

where C and R_1 are shown in Fig. 4. Thus, the relationship between frequency and temperature is linearized by selecting the appropriate R_1 . This design does not require any extra bias voltage. Besides, it uses fewer resistors to reduce errors caused by resistor variation. However, poor sensitivity leads to design difficulty of the back-end readout circuit.

Sonowal and Bhuyan [8] proposed a thermistor sensor that employs piecewise linear interpolation implemented by an FPGA as shown in Fig. 5. The output voltage curve of the voltage divider is divided into many segments. Then, the FPGA determines the segment the voltage is located in to derive the temperature. However, the FPGA requires massive data computation to converge. Thus, disadvantages are extra memory as well as high computation cost. A similar method can also be found in [9].

The thermistor sensor is a good choice according to Table I, but Bosson *et al.* show that the resistance does not have a linear relationship with the temperature. Nevertheless, none of these methods are unable to resolve the trade-off between linearization and design complexity. Therefore, this paper proposes a simple architecture with a temperature-to-frequency converter to increase the sensitivity and reduce the error rate.

In general, digital temperature sensors can be classified into two categories: voltage-domain temperature sensor and time-domain temperature sensor. They have their own temperature

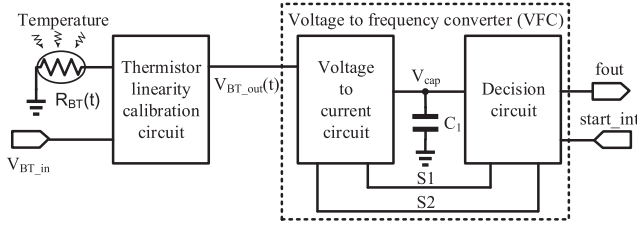


Fig. 6. Block diagram of the proposed temperature-to-frequency converter.

sensing components, respectively, to attain an analog signal with respect to the temperature variation. The analog signal will be converted to digital signal through a voltage-to-digital converter (ADC) or time-to-digital converter (TDC). Because the thermistor sense is one kind of voltage-domain temperature sensors, the voltage to frequency converters (VFC) is selected as a converter. The VFC is a popular choice for many electronic control and measurement systems, e.g., [10]. In measurement systems, the sensing voltage is drastically affected by noise, which results in unacceptable accuracy. The VFC is able to convert the sensed voltage into a ratio-metric frequency with great noise immunity. Besides, to ensure conversion accuracy, the ratio-metric frequency should be a reliable function of the corresponding sensed voltage. Thus, sensitivity, bandwidth, and linearity become quality factors of the VFC. A good ratio-metric frequency of the VFC provides insightful information regarding the selection of passive or active elements, which also play a role as sensors [11]–[13].

Since the ocean is considered as the most abundant natural resource on the earth, many countries are developing autonomous underwater vehicles (AUV) to explore this territory. Battery module system of AUV is the main power source to carry out underwater tasks with the efficiency and safety. Notably, the temperature significantly affects the charge and discharge of the batteries. The temperature of the sea water is from 0 °C to 24 °C [14]. Meanwhile, AUV may generate waste heat during operations. Therefore, a high-linearity voltage-to-frequency device for linear calibration of the thermistor sensor for battery monitoring in the [−5 °C, 40 °C], which is wider than the mentioned temperature range, is proposed in this work to monitor the temperature around batteries, as shown in Fig. 6. A detailed schematic and analysis of the proposed design is given in Section II. Section III describes detailed measurement results to that demonstrate the performance of the thermistor linearity calibration circuit and the VFC design. Conclusions are drawn in Section IV.

II. ARCHITECTURE OF PROPOSED TEMPERATURE-TO-FREQUENCY CONVERTER

With reference to Fig. 6 again, a temperature-to-frequency converter is composed of a thermistor linearity calibration circuit, a voltage-to-current circuit, and a decision circuit. Because the characteristic function of the thermistor, $R_{BT}(t)$, is nonlinear, we add a thermistor linearity calibration circuit to carry out predictable linearization. However, the output signal of the Thermistor linearity calibration circuit is seriously affected by supply voltage variation and the associated noise

coupled with it. Hence, we propose to take advantage of a VFC composed of a voltage-to-current circuit and decision circuit converting the output of the thermistor linearity calibration circuit into a signal with a ratio-metric frequency. All of the sub-circuits in Fig. 6 will be analyzed and designed theoretically in the following text.

A. Thermistor Linearity Calibration Circuit

The thermistor linearity calibration circuit is composed of two resistors, R_{cal} and R_f , and an opamp as shown in Fig. 7, where V_{BT_in} is an external DC bias. The thermistor linearity calibration circuit is used to enlarge the range of the sensing voltage and reject the noise coupled from the following circuitry. The resistance of the thermistor is shown in Eqn. (4) [15]:

$$R_{BT}(t) = R_0 e^{\beta \left(\frac{1}{t} - \frac{1}{t_0} \right)} \quad (4)$$

where R_0 is the resistance of the thermistor at 298.15°K, β is the temperature constant of the thermistor, t is the sensed temperature, and t_0 is 298.15°K. $V_{BT_out}(t)$ is derived as Eqn. (5):

$$V_{BT_out}(t) = V_{BT_in} \times \left[1 + \frac{R_f}{R_{BT}(t) + R_{cal}} \right] \quad (5)$$

where R_{cal} is a resistor for calibration, and R_f is a feedback resistor. The Taylor series expansion of Eqn. (5) is derived to obtain the following result:

$$\begin{aligned} V_{BT_out}(t) &= V_{BT_out}(t_m) + (t - t_m) V'_{BT_out}(t_m) \\ &+ \frac{(t - t_m)^2}{2!} V''_{BT_out}(t_m) + \frac{(t - t_m)^3}{3!} V'''_{BT_out}(t_m) + \dots \end{aligned} \quad (6)$$

where t_m is the central temperature of the selected temperature range. After truncating all the terms except the first three terms, $V_{BT_out}(t)$ is reorganized as

$$\begin{aligned} V_{BT_out}(t) &= V_{BT_out}(t_m) + (t - t_m) V'_{BT_out}(t_m) \\ &+ \frac{(t - t_m)^2}{2!} V''_{BT_out}(t_m) \end{aligned} \quad (7)$$

Therefore, the coefficient of the quadratic term needs to be nullified for linearization, which is expressed as Eqn. (8):

$$\begin{aligned} \frac{d^2}{dt^2} V_{BT_out}(t) \Big|_{t=t_m} &= \frac{d^2}{dt^2} \left\{ V_{BT_in} \times \left[1 + \frac{R_f}{R_{BT}(t) + R_{cal}} \right] \right\} = 0 \end{aligned} \quad (8)$$

Because V_{BT_in} is a constant, we only need to deal with the rightmost term. Assume $f(t)$ is defined as follows:

$$f(t) = 1 + \frac{R_f}{R_{BT}(t) + R_{cal}} \quad (9)$$

The quadratic differential of Eqn. (9) becomes Eqn. (10):

$$\begin{aligned} \frac{d^2}{dt^2} f(t) \Big|_{t=t_m} &= \frac{R_f [R_{cal} + R_{BT}(t_m) R''_{BT}(t_m) - 2R'_{BT}(t_m)^2]}{[R_{cal} + R_{BT}(t_m)]^3} \Big|_{t=t_m} = 0 \end{aligned} \quad (10)$$

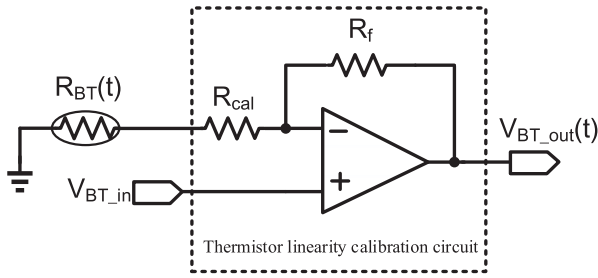


Fig. 7. Schematic of thermistor linearity calibration circuit.

When Eqn. (10) holds, the numerator must be zero as follows:

$$R_{cal} + R_{BT}(t_m)R''_{BT}(t_m) - 2R'_{BT}(t_m)^2 = 0 \quad (11)$$

R_{cal} is then derived as follows:

$$R_{cal} = \frac{2R'^2_{BT}(t_m)}{R''_{BT}(t_m)} - R_{BT}(t_m) \quad (12)$$

Using Eqn. (4), R_{cal} is reorganized as

$$R_{cal} = \frac{\beta - 2 \cdot t_m}{\beta + 2 \cdot t_m} \times R_{BT}(t_m) \quad (13)$$

Thus, the coefficient of the quadratic term can be made 0 by selecting R_{cal} with an appropriate resistance. In sum, the first step is to select the temperature range to detect, and then choose the center temperature to plug into Eqn. (12) to derive R_{cal} . Finally, a thermistor, two resistors, and an opamp comprising the non-inverting amplifier are able to linearize the function of the sensing voltage.

B. Voltage-to-Frequency Converter

The VFC in Fig. 6 is responsible for converting the linearization of the sensed voltage ($V_{BT_out}(t)$) to a digital pulse train with corresponding frequency. The VFC consists of a voltage-to-current circuit and a decision circuit, which will be introduced in the following text.

C. Voltage-to-Current Circuit

In the voltage-to-current circuit, a reference current (I_{ref}) is generated by the left-hand-side circuit in Fig. 8, where an opamp, and a resistor, R_s are used. The improved high-swing cascode current mirror composed of MP3 ~ MP9, MP14, and MN2 ~ MN7 eliminates the channel length modulation and drain-induced threshold shift to provide a highly accurate mirroring current [16]. Therefore, I_{ref} is written as follows:

$$I_{ref} = \frac{V_{BT_out}(t)}{R_s} \quad (14)$$

Because the W/L ratio of MP1 and MP3 is selected to be K , the current of MP3 is I_{ref}/K . The current mirror composed of MP3 ~ MP9, MP14, and MN2 ~ MN7 in Fig. 8 duplicates $1/K$ times of I_{ref} to I_x as follows:

$$I_x = \frac{I_{ref}}{K} = \frac{V_{BT_out}(t)}{K \times R_s} \quad (15)$$

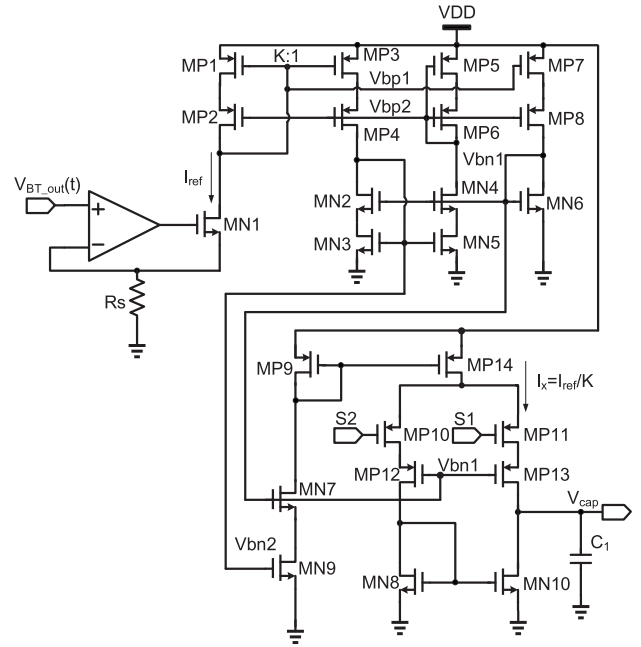


Fig. 8. Schematic of voltage-to-current circuit.

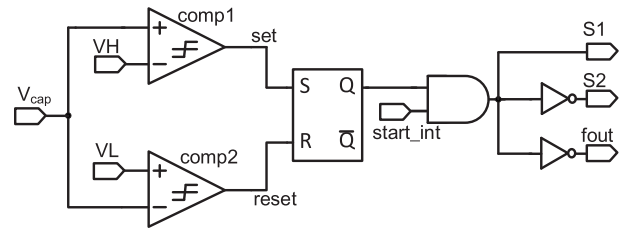


Fig. 9. Schematic of decision circuit.

Thus, the I_x current charges or discharges the capacitor (C_1) depending on the controlled signals ($S1$ and $S2$) to generate a voltage (V_{cap}). Notably, $S1$ and $S2$ are generated from the following decision circuit.

D. Decision Circuit

The decision circuit in Fig. 6 consists of two comparators, one SR latch, one AND gate, and two inverters, as shown in Fig. 9. When the system starts, $start_int$ is reset low to make the voltage-to-current circuit charge C_1 . Then, because V_{cap} is continuously increased and is finally higher than VH , $comp1$ will be pulled high while $comp2$ will be pulled low. Furthermore, SR_out is pulled high and $start_int$ turns high. Therefore, $S1$ is pulled high to turn off MP11 (in Fig. 8), and $S2$ is pulled low to turn on MP10 (in Fig. 8). The discharging current of C_1 equals I_x . By contrast, when V_{cap} is smaller than VL , the scenario becomes the opposite of the above operation. The voltage-to-current circuit charges C_1 with I_x again to increase V_{cap} . The waveforms of those signals in the decision circuit are shown in Fig. 10. The above steps are iterated to generate a digital pulse signal with a frequency (f_{out}) as follows:

$$f_{out} = \frac{I_x}{2C_1(VH-VL)} \quad (16)$$

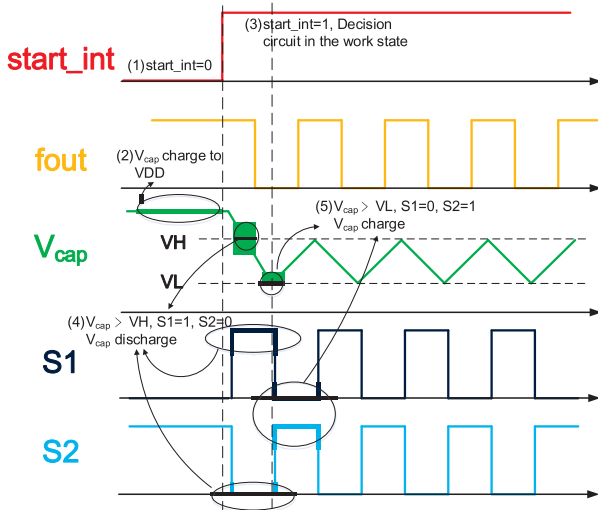


Fig. 10. Waveforms of signals in decision circuit.

TABLE II

THE RESULT OF LINEARIZATION APPLIED TO DIFFERENT THERMISTORS BY THE PROPOSED METHOD AND EQUATIONS

Thermistor	β	R_f (k)	R_{cal} (k)	Before linearization (%)	After linearization (%)
B57861S103J40	3988	30	11.74	90.5	99.91
B57861S0104	4540	100	76.78	88.86	99.56
B57861S0503	3760	100	36.31	91.46	99.75

From Eqn. (5) and Eqn. (15), f_{out} can be derived as

$$f_{out} = V_{BT_in} \times \frac{[1 + \frac{R_f}{R_{BT}(t) + R_{cal}}]}{2C_1(VH-VL)K \times R_s} \quad (17)$$

On the basis of Eqn. (17), $R_{BT}(t)$ is reorganized as follows:

$$R_{BT}(t) = \frac{V_{BT_in} \times R_f}{2C_1(VH-VL)K \times R_s \times f_{out} - V_{BT_in}} - R_{cal} \quad (18)$$

On the basis of Eqn. (4), the temperature (t) can be indirectly estimated using $R_{BT}(t)$:

$$t = \frac{1}{\frac{\ln(\frac{R_{BT}(t)}{R_0})}{\beta} + \frac{1}{t_0}} \quad (19)$$

To justify the functionality of linearizing by our method, we apply the proposed method (Eqn. (18)) on three thermistors and the appropriate R_{cal} derived by Eqn. (13) as shown in Table II. The linearities of all these three different thermistors are all calibrated to be over 99% in the $[-5^\circ\text{C}, 40^\circ\text{C}]$ by the proposed method and equations therewith.

III. IMPLEMENTATION AND MEASUREMENT

The proposed temperature to frequency converter with the linearization circuit for the thermistor is implemented using a TSMC 0.5 μm CMOS high voltage mixed signal based LDMOS USGAL 2P3M polycide (T50UHV). Fig. 11 shows the layout and die photo of the proposed converter. The area of the entire chip is $1577.67 \times 1515.79 \mu\text{m}^2$, and its core area is

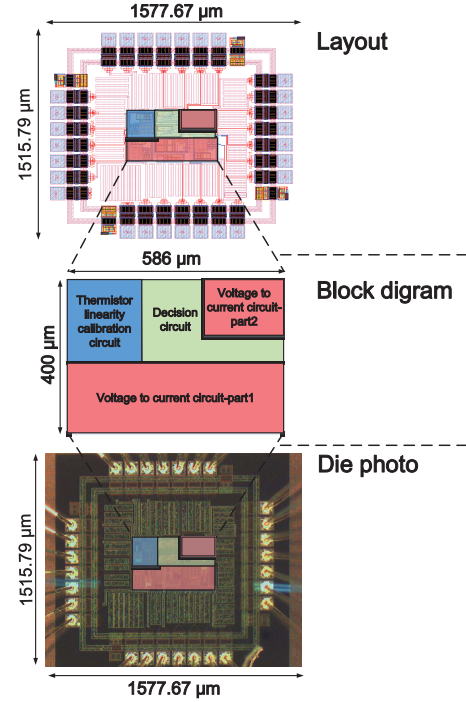


Fig. 11. Layout and die photo of the proposed temperature-to-frequency converter.

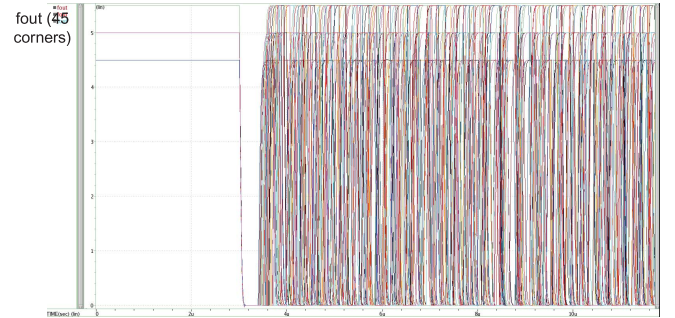


Fig. 12. All-PVT-corner post-layout simulation results.

$586 \times 400 \mu\text{m}^2$. The all-PVT-corner post-layout simulation of the proposed converter is shown in Fig. 12. When the sensing temperature range is $268.15 \sim 313.15^\circ\text{K}$ ($-5 \sim 40^\circ\text{C}$), the proposed converter has the worst-case linearity error of 1.42% when the corner in SS process, VDD is -10% VDD, and the temperature is 25°C as shown in Fig. 13. Besides, the worst sensing error is -1.04°C , and the average error is 0.37°C , as shown in Fig. 14.

The measurement of the proposed design on silicon is shown in Fig. 15. The thermistor is placed in the programmable compact temperature and humidity chamber (TERCHY MHK-120). The power supply (Rohde and Schwarz E3631A DC Power Supply) generates the supply voltage. The oscilloscope (Agilent 54855A) is used to display f_{out} .

To ensure that the proposed chip is functional in the range $268.15 \sim 313.15^\circ\text{K}$, the power supply is applied to provide 10 temperature cases, i.e., $268.15, 273.15, 278.15, \dots, 313.15^\circ\text{K}$. The measurement results of the temperature sensor are summarized in Table III, and the

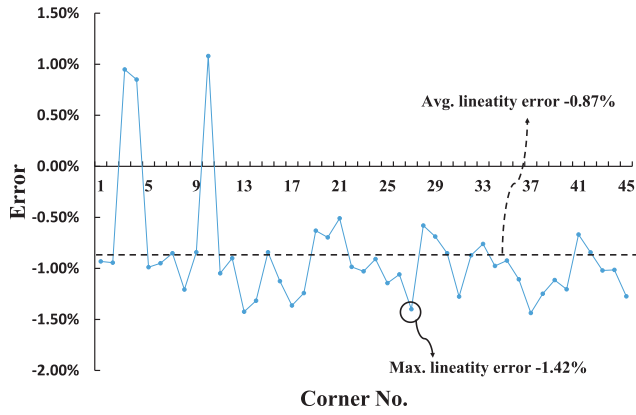


Fig. 13. Linearity error of all-PVT-corner post-layout simulation results.

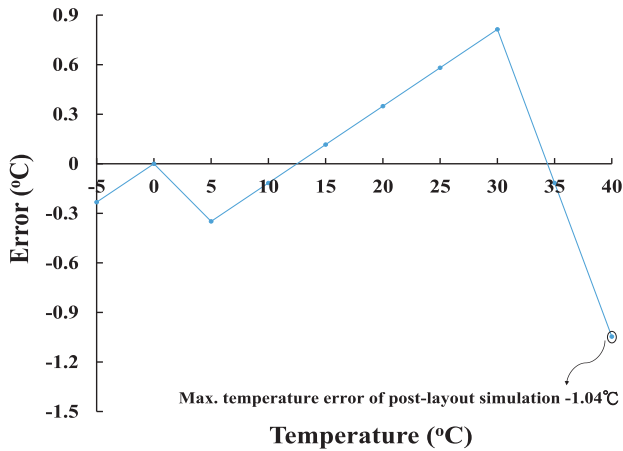


Fig. 14. Sensing temperature error distribution of all-PVT-corner post-layout simulation results.

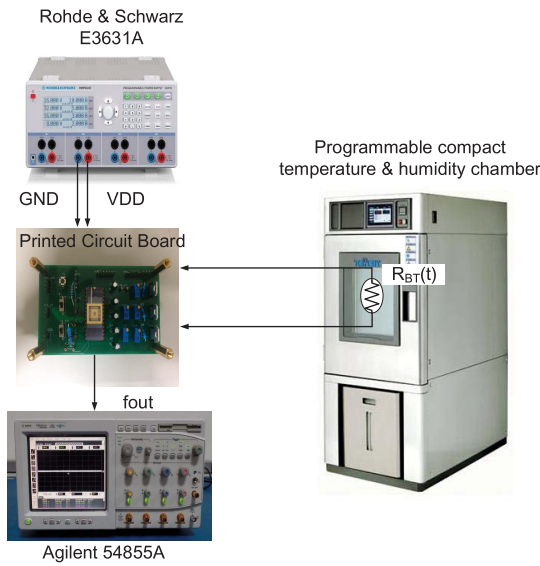


Fig. 15. Measurement setup of the proposed temperature sensor.

TABLE III
THE MEASUREMENT RESULTS OF THE TEMPERATURE SENSOR

Real temperature (°K)	fout (MHz)	Derived temperature (°K)	Temperature error (%)	Linearity error (%)
268.15	1.6183	267.3236	-0.31	-0.50
273.15	1.6854	272.4577	-0.25	0.07
278.15	1.7658	278.0057	-0.05	0.19
283.15	1.8561	283.811	0.23	0.06
288.15	1.9478	289.5231	0.48	-0.18
293.15	2.0355	295.021	0.64	-0.41
298.15	2.1012	299.2772	0.38	-0.51
303.15	2.1637	303.5254	0.12	-0.47
308.15	2.2223	307.7709	-0.12	-0.08
313.15	2.2705	311.5266	-0.52	0.50

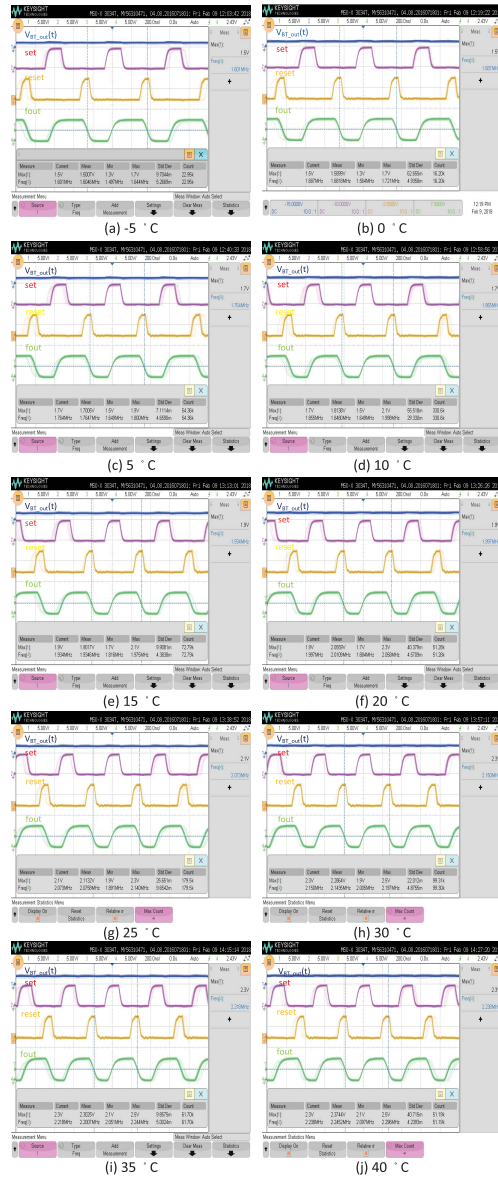


Fig. 16. Timing measurement results of the proposed temperature sensor. (a) -5 °C. (b) 0 °C. (c) 5 °C. (d) 10 °C. (e) 15 °C. (f) 20 °C. (g) 25 °C. (h) 30 °C. (i) 35 °C. (j) 40 °C.

digital output waveforms are shown in Fig. 16. When the sensing temperature range is 268.15 ~ 313.15°K, the output range of the Temperature sensor, fout, is 1.62 ~ 2.27 MHz.

Fig. 17 summarizes the measurement results of fout. The maximum error with respect to a linear asymptotic line is low as ±0.5%.

TABLE IV
PERFORMANCE COMPARISON OF TEMPERATURE SENSORS

	[7] TIM	[17] ISIE	[18] ICPEICES	[4] SJ	[19] HNICEM	[20] TBCS	[21] SJ	[22] ST	This work
Year	2009	2010	2016	2016	2017	2018	2017	2008	2018
Implementation	PCB	180 μm CMOS	PCB	PCB	PCB	prototype	65 μm CMOS	discretes	T50UHV CMOS
Power (mW)	N/A	0.5	N/A	N/A	N/A	1.58	53 (μW)	15	11
Output frequency (kHz)	1 ~ 7.5	0 ~ 2000	0 ~ 50	N/A	0 ~ 10 (Hz)	5 ~ 10 (Hz)	1.83	N/A	500 ~ 2200
VFC input range (V)	N/A	0 ~ 1.6	N/A	N/A	N/A	N/A	N/A	N/A	0.5 ~ 2.5
Linearity error (%)	1	2	4.61	1	9.05	1.017	N/A	N/A	± 0.5
Sensitivity (kHz/V)	N/A	1250	N/A	N/A	N/A	N/A	N/A	N/A	850
Temperature range ($^{\circ}\text{C}$)	0 ~ 120	0 ~ 80	0 ~ 100	30 ~ 120	-10 ~ 100	30 ~ 42	30 ~ 70	-40 ~ 100	-5 ~ 40
Temperature error (%)	3	8	5	3	4.204	4	8	3.8	1.47($\leq \pm 3\sigma$)
FOM ^b	40	10	20	30	26.17	3	5	36.84	37.41

Note: ^bFOM = Temperature range/Temperature error

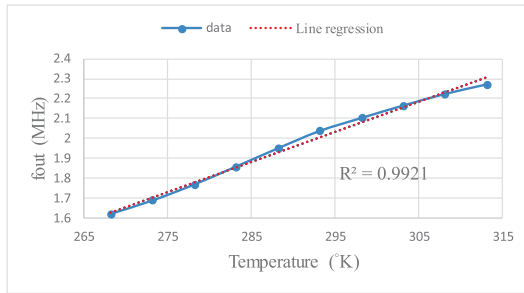


Fig. 17. Measurement result of f_{out} at $-268.15 \sim 313.15^{\circ}\text{C}$.

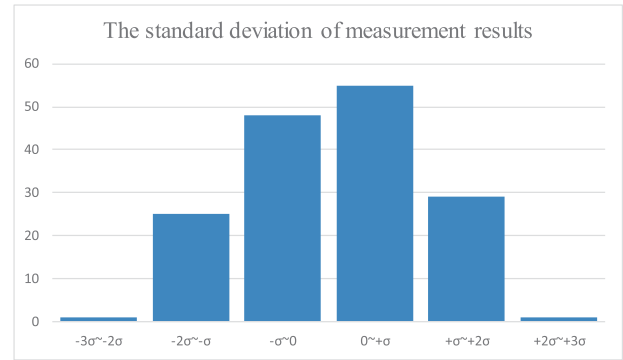


Fig. 20. Standard deviation distribution of measurement results.

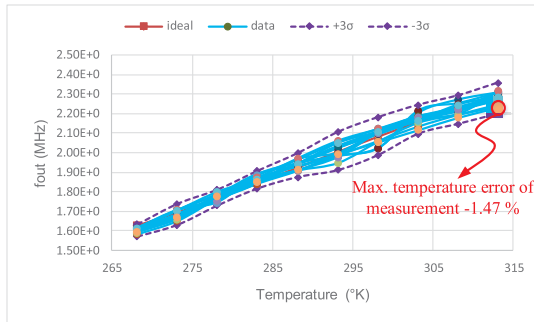


Fig. 18. Statistics of measurement results of proposed temperature sensor.

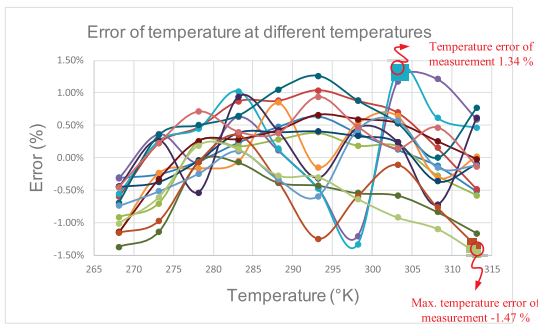


Fig. 19. Sensing temperature error of the proposed temperature sensor.

Three chips of the proposed Temperature sensor are used to run six temperature measurements five times for each chip. These measurement results are summarized in Fig. 18. The

theoretical sensing temperature is derived from f_{out} on the basis of Eqn. (17). Next, the error of the sensed temperature compared with the real temperature is shown in Fig. 19. The maximum error with respect to the ideal line is as low as -1.47% . The standard deviation of measurement results is smaller than $\pm 3\sigma$ as shown in Fig. 20.

The performance comparison of the proposed design with the design described in several recent works is tabulated in Table IV. Notably, the proposed design is the only solution that generates a digital signal (frequency) without using an ADC. In addition, the proposed design works in the range $268.15 \sim 313.15^{\circ}\text{K}$, with a maximum error of approximately 1.47% , which is the best result achieved to date.

IV. CONCLUSION

In this paper, a temperature-to-frequency converter with linearity calibration is proposed. A detailed schematic design and analysis of the proposed design are given as well. The proposed design can be adapted to different thermistors as long as the appropriate R_{cal} based on Eqn. (13) is selected. That is, any nonlinear thermistor can be calibrated to attain high linearity by the proposed method. The measurement results of thermistor linearized by our method demonstrate a high linearity, where the linearity error is smaller than $\pm 0.5\%$. Besides, not only are the sensitivity and the output frequency enhanced, the temperature error, which is less than 1.47% , is also better than that of the traditional temperature sensors.

Moreover, this work converts the sensed voltage into a digital signal (frequency) without using an ADC. The digital signal denoting temperature can be used in many applications, e.g., the parameters for calculating SOC of the battery system.

REFERENCES

- [1] G. Bosson, F. Guttman, and L. M. Simmons, "Relationship between temperature and resistance of a thermistor," *J. Appl. Phys.*, vol. 21, no. 12, pp. 1267–1268, Dec. 1950.
- [2] *NTC Thermistors for Temperature Measurement*, TDK, Tokyo, Japan, 2018.
- [3] E. O. Doebelin, *Measurement Systems: Application and Design*. New York, NY, USA: McGraw-Hill, 1990.
- [4] A. R. Sarkar, D. Dey, and S. Munshi, "Linearization of NTC thermistor characteristic using op-amp based inverting amplifier," *IEEE Sensors J.*, vol. 13, no. 12, pp. 4621–4626, Dec. 2013.
- [5] S. Bandyopadhyay, A. Das, A. Mukherjee, D. Dey, B. Bhattacharyya, and S. Munshi, "A linearization scheme for thermistor-based sensing in biomedical studies," *IEEE Sensors J.*, vol. 16, no. 3, pp. 603–609, Feb. 2016.
- [6] V. N. Kumar, K. V. L. Narayana, A. Bhujangarao, and S. Sankar, "Development of an ANN-based linearization technique for the VCO thermistor circuit," *IEEE Sensors J.*, vol. 15, no. 2, pp. 886–894, Feb. 2015.
- [7] Z. P. Nenova and T. G. Nenov, "Linearization circuit of the thermistor connection," *IEEE Trans. Instrum. Meas.*, vol. 58, no. 2, pp. 441–449, Feb. 2009.
- [8] D. Sonowal and M. Bhuyan, "Linearizing thermistor characteristics by piecewise linear interpolation in real time FPGA," in *Proc. Int. Conf. Adv. Comput., Commun. Inform. (ICACCI)*, Aug. 2013, pp. 1976–1980.
- [9] A. Burke, "Linearizing thermistors with a single resistor," *Electronics*, vol. 54, no. 11, pp. 151–154, 1981.
- [10] G. C. M. Meijer, *Smart Sensor Systems*. New York, NY, USA: Wiley, 2008.
- [11] S. Cai and I. M. Filanovsky, "High precision voltage-to-frequency converter," in *Proc. IEEE Midwest Symp. Circuits Syst. (MWSCAS)*, vol. 2, Aug. 1994, pp. 1141–1144.
- [12] K. Allidina, M. A. Taghvaei, F. Nabki, P.-V. Cicek, and M. N. El-Gamal, "A MEMS-based vacuum sensor with a PLL frequency-to-voltage converter," in *Proc. IEEE Int. Conf. Electron., Circuits Syst. (ICECS)*, Dec. 2009, pp. 583–586.
- [13] B. Calvo, N. Medrano, S. Celma, and M. T. Sanz, "A low-power high-sensitivity CMOS voltage-to-frequency converter," in *Proc. IEEE Int. Midwest Symp. Circuits Syst. (IMSCS)*, pp. 118–121, Aug. 2009.
- [14] J. Bergman. (Feb. 2011). *Temperature of Ocean Water*. [Online]. Available: <https://www.windows2universe.org/earth/Water/temp.html>
- [15] J. S. Steinhart and S. R. Hart, "Calibration curves for thermistors," *Deep Sea Res. Oceanogr. Abstracts*, vol. 15, no. 4, pp. 497–503, Aug. 1968.
- [16] P. E. Allen and D. R. Holberg, *CMOS Analog Circuit Design*. London, U.K.: Oxford Univ. Press, 2011.
- [17] B. Calvo, C. Azcona, N. Medrano, and S. Celma, "A low-cost VFC for low-power sensor interfaces," in *Proc. IEEE Int. Symp. Ind. Electron. (ISIE)*, Jul. 2010, pp. 379–383.
- [18] K. P. S. Rana, V. Kumar, and T. Prasad, "Enhancing linearity in thermistor signal conditioning circuit using linear numerical search," in *Proc. IEEE Int. Conf. Power Electron., Intell. Control Energy Syst. (ICPEICES)*, Jul. 2016, pp. 1–6.
- [19] R. S. Concepcion, F. R. G. Cruz, F. A. A. Uy, J. M. E. Baltazar, J. N. Carpio, and K. G. Tolentino, "Triaxial MEMS digital accelerometer and temperature sensor calibration techniques for structural health monitoring of reinforced concrete bridge laboratory test platform," in *Proc. IEEE Int. Conf. Humanoid, Nanotechnol., Inf. Technol., Commun. Control, Environ. Manage. (HNICEM)*, Dec. 2017, pp. 1–6.
- [20] S. S. Karipott, P. M. Veetil, B. D. Nelson, R. E. Guldberg, and K. G. Ong, "An embedded wireless temperature sensor for orthopedic implants," *IEEE Sensors J.*, vol. 18, no. 3, pp. 1265–1272, Feb. 2018.
- [21] A. Kobayashi *et al.*, "Design and experimental verification of a 0.19 V 53 μ W 65 nm CMOS integrated supply-sensing sensor with a supply-insensitive temperature sensor and an inductive-coupling transmitter for a self-powered bio-sensing system using a biofuel cell," *IEEE Trans. Biomed. Circuits Syst.*, vol. 11, no. 6, pp. 1313–1323, Dec. 2017.
- [22] *Precision Temperature Sensors LM335*, ST Microelectron., Geneva, Switzerland, 2008.

Chua-Chin Wang, photograph and biography not available at the time of publication.

Zong-You Hou, photograph and biography not available at the time of publication.

Jhieh-Cheng You, photograph and biography not available at the time of publication.